Abschlussbericht zum Max-Buchner-Forschungsstipendium

MBFSt-Kennziffer: 3354, Förderperiode 07/2013 – 06/2014

Substitution of platinum by laser-generated nickel-alloy nanoparticles for heterogeneous catalysis

M.Sc. Galina Marzun, Dr. Philipp Wagener

University of Duisburg-Essen

Technical Chemistry I and Center for Nanointegration Duisburg-Essen (CENIDE)

NanoEnergieTechnikZentrum (NETZ)

Abstract

Platinum is a scarce and expensive metal that is mostly used as a catalytic active material for energy converting devices like fuel cells. The more cost-effective metal nickel and its alloys are an interesting alternative to platinum. For this purpose, we fabricated ligand-free and purely electrostatically stabilized nickel-molybdenum nanoparticles by laser ablation in liquid and characterized their chemical properties using TEM-EDX, XRD, optical and electrochemical methods.

Introduction

Bi-metallic alloy nanoparticles reveal altered properties compared to mono-metal nanoparticles. Hence, they are of high interests and importance for several applications, such as biomedicine, microelectronics and catalysis, which is spread over a large range of sub-areas [1] [2] [3]. Several studies have shown that catalysts containing alloy nanoparticles improve the catalytic activities for the electroreduction of dioxygen which is a key reaction in proton exchange membrane fuel cell (PEMFC) [4] [5] [6].

Platinum is well-known as an essential material for electro catalysts in fuel cells [7] [8] [9] [10]. It is the most effective catalyst for the oxidation of hydrogen and the reduction of oxygen [11] [12]. Also for the hydrogen evolution reaction (HER), which plays an important role in the electro- and photocatalysis [13], platinum shows the highest catalytic activity [14], but it is also an expensive and scarce metal. Considering the volcano plot, where the exchange currents for the HER is plotted vs. the strength of a metal-hydrogen bond, nickel is the most active non-novel metal [14] [15]. Because of the high current densities, a considerably lower price and a better availability, nickel shows a high potential for the production of highly active electro-catalysts.

Nanoparticle generation by pulsed laser ablation in liquid is a technology with a high future impact on technical and medical applications, where a variety of solvents [16] [17] [18] and materials [19] [20] [21] can be used for the nanoparticle production [22]. In contrast to chemical synthesis methods for nanoparticles, laser ablation do not require any precursors, which often contribute to impurities in colloids [23]. By this method alloy nanoparticles can be produced by ablating of a target, which is made by pressing a powder of mixed materials, where any desired material and composition can be attained [21] [24].

In our study, we synthesized and characterized bimetallic nanoparticles consisting of nickel and molybdenum as an electro catalyst for fuel cells. The nanoparticles were synthesized by pulsed laser ablation of a pressed micro-powder immersed in water.

Experimental Details

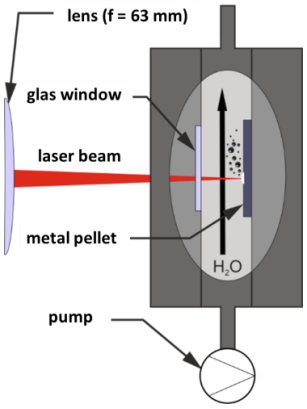

Figure 1: experimental setup, showing ablation flow chamber

Colloidal nanoparticles were prepared by pulsed laser ablation of the targets in a self-made flow-through chamber using a Nd:YAG nanosecond-laser at a fundamental wavelength of 1064 nm with a repetition rate of 5 kHz and a pulse energy of 6.4 mJ. The laser beam was focused and scanned in a spiral pattern onto the target during deionized water was flowed through the chamber (Figure 1).

For the preparation of the targets, nickel and molybdenum micro-powders at different molar ratios were mixed and pressed at 100 kN and the formed targets were sintered at 800 °C for 1 hour under argon atmosphere, for a higher mechanical stability.

Laser-generated nanoparticles were characterized by UV-VIS spectroscopy, grazing incidence X-ray (GIXRD), transmission electron microscopy (TEM) and energy disperse X-ray spectroscopy (EDX). Electrochemical measurements were carried out in a three electrode electrochemical cell at room temperature, using a glassy carbon electrode loaded with nanoparticles as working electrode. Cyclic voltammograms were recorded with a scan rate of 100 mV/s in a range of -0.9 V to 0.75 V using an Ag/AgCl-reference electrode in a saturated KCl solution, a platinum wire as the counter electrode and a 1 M NaOH as electrolyte solution, which was purged with nitrogen.

Results and discussion

Analyzing colloidal nanoparticles by optical methods can reveal a plenty of information of their chemical properties. Pulsed laser ablation yields of target of different compositions yields in colored colloids. Figure 2 shows the UV-VIS spectra of the nanoparticles with several molar ratio. The binary colloids show a target dependent optical behaviour. By decreasing the molar fraction of nickel in the pressed micropowder, the broad absorption in the colloids caused by nickel decreases and tends to molybdenum like absorption spectra.

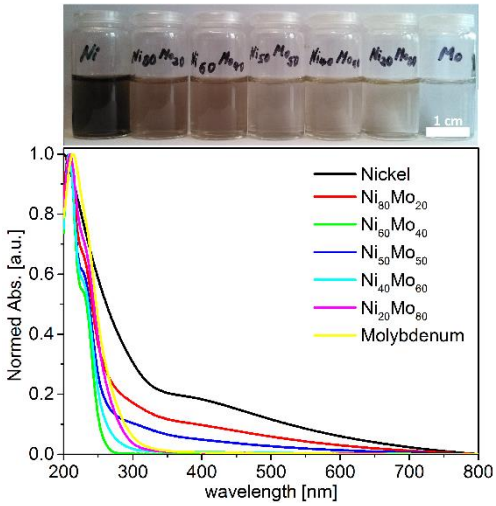

Figure 2: Colloids with several metallic composition and the respective UV-Vis absorption spectra

The absorption spectra of pure nickel-colloid exhibit a broad absorption in the UV region, which is consistent with chemically prepared nickel nanoparticles [25]. Metallic nickel nanoparticles were obtained by laser ablation in water [26] [27]. The UV-Vis spectra of molybdenum colloids shows a strong absorption peak at about 215 nm corresponding to MoO_3, that is caused by an interband transition in the $(MoO_6)^{6-}$ octahedron where Mo^{5+} is generated by capturing electron by Mo^{6+} [28], [29]. The absorption shoulder at 240 nm indicates the presence of MoO_4^{2-} and $HMoO_4^-$ [30] [31] (Figure 3). Typically absorption band of metallic molybdenum was not observed [27].

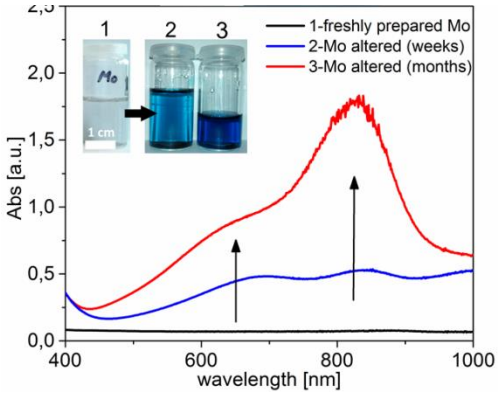

Figure 3: UV-Vis spectra of freshly prepared molybdenum (1) compared to altered colloids after a few weeks (2) and months (3)

After a few weeks, the colour of the colloids containing molybdenum turns to blue and some absorption bands in the range of 500-900 nm appears (Figure 1, right), which indicates a continuous oxidation after the ablation process. The blue colour can be attributed to the semi-conductive properties of MoO_3 ($E_g \geq 2.9$ eV) [32] [33]. By irradiation with UV light excitons are generated, where the reaction of adsorbed water

with holes leads to a proton release, which then reacts with molybdenum oxide and a charge transfer causes the colouration of the colloids [32], [33].

TEM analysis were performed to investigate the average size and the morphology of the nanoparticles. As can be seen in Figure 4 the nanoparticles are spherical and showing a log-normal size distribution, which is in accordance with the literature handling with laser-generated nanoparticles [34] [35] [36]. The average nanoparticle diameter fluctuates with the metal ratio set in the targets, where the bimetallic colloids contain larger nanoparticles compared to the pure colloids. Similar observations were made by Sarker et al., where the nanoparticle size of binary and ternary alloy nanoparticles varied with the molar ratio of metals produced by laser irradiation [37] [38]. The results were not described in detail so far, but they suppose this tendency is due to differences of surface energy, interatomic distance and atomic ratio [38] [39].

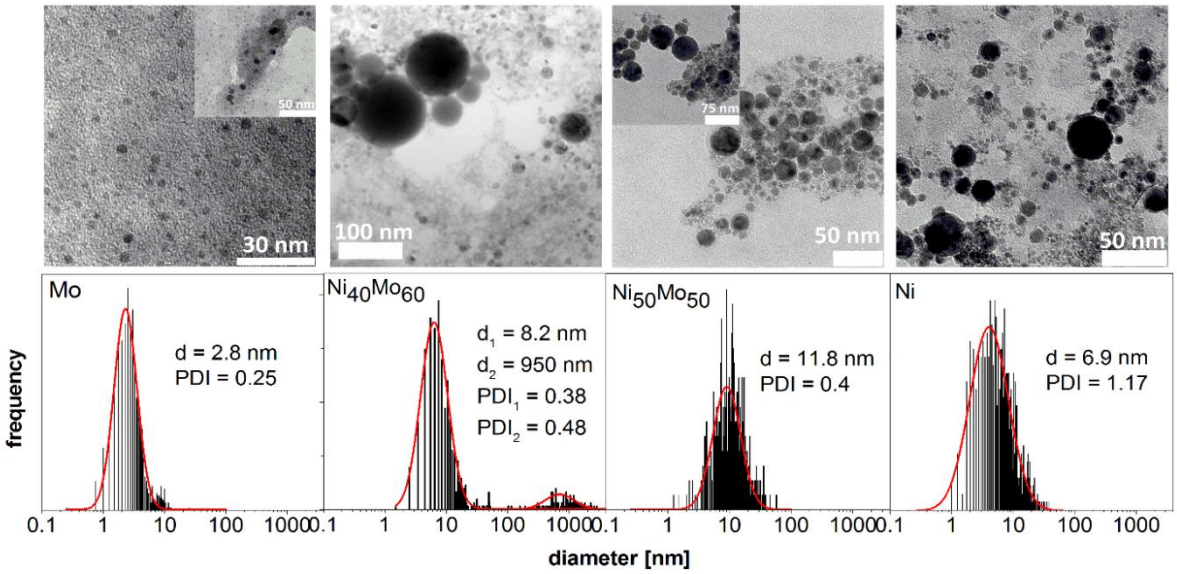

Figure 4: TEM-mirographs of pure molybdenum, nickel and the colloids ablated from the targets with a molar fraction ration for nickel-molybdenum of 40:60 and 50:50.

To analyse the elemental distribution of the nanoparticles, TEM-EDX line scans were carried out with the $Ni_{40}Mo_{60}$-colloid of randomly chosen nanoparticles. Both elements were detected in the spectra. We could find that the elemental composition is not consistent for all nanoparticles and varies with the nanoparticle size (Figure 5). The large nanoparticles (2nd mode) are molybdenum-rich, whereas smaller nanoparticles consist of nickel. Deviation in the stoichiometry of laser-generated Cu/Zn nanoparticles has been observed by Koch et al., where the use of a nanosecond laser and higher laser fluences yielded to an increased formation of polydisperse particles up to micrometer range [40]. Different simultaneous ablation processes and ejection kinetics of the metals may lead to deviations in the composition of the laser-generated nanoparticles, where the energy density deposited on the target plays an important role in the nanoparticle formation [41] [42] [35]. Due to the high laser fluences (81 J/cm^2) applied in our

experiment, we assume that multiple ablation mechanisms like fragmentation, vaporisation and phase explosion are responsible for nanoparticle formation, that lead to a broad size distribution [35].

A good agreement of the elemental composition with the targets can be found in the literature for alloy nanoparticles consisting of noble metals like PtAu, AuAg and PtIr [21] [43] [44]. However it was reported, that the stoichiometry of other metals like SmCo differs from the target, which was explained due to a large different in the heat of evaporation of the both metals [45]. Amendola et al. concluded from this and other works, that the stoichiometry of alloy nanoparticles is more influenced by different reactivity with the solvent and oxygen molecules, than the heat of evaporation (Δ_H) [35]. This was explained by the fact, that the stoichiometry of laser-generated FePt alloy nanoparticles were not retained as in the target and varies with the chosen solvent in Ref. [46] and [35]. In our study, we used water as a solvent during the laser ablation. Since oxygen is good soluble in water, oxidation of the non-noble metal nanoparticles can take place. That oxidized molybdenum nanoparticles are present was shown in the UV-VIS spectra of the colloids (Figure 3).

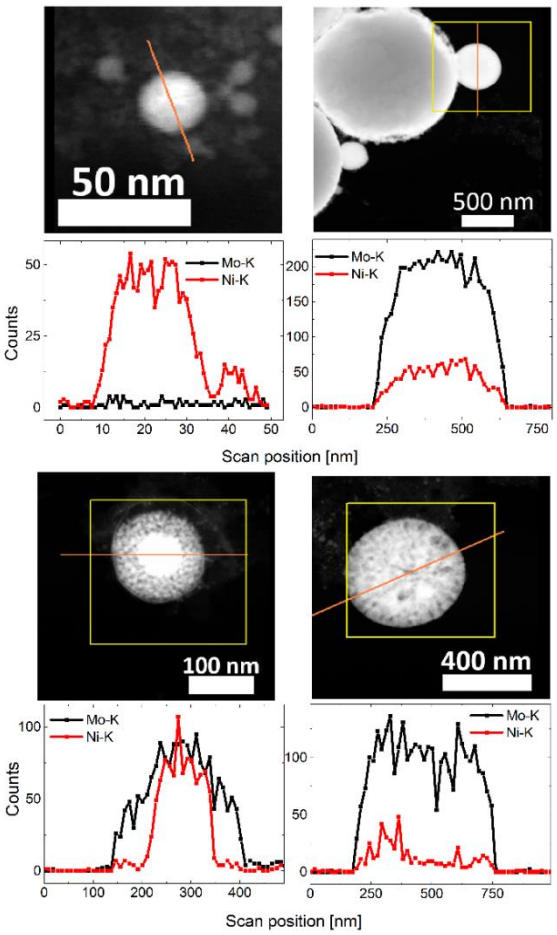

Figure 5: TEM-EDX line scans of a nickel-molybdenum colloid ablated from a target with a molar fraction ratio for nickel-molybdenum of 40:60

For more detailed structural analysis, XRD measurements were performed. Figure 6 shows the typical diffractograms, where additionally to the characteristic fcc-peaks of nickel, pronounced nickel oxide (NiO)-peaks were detected in the nickel colloid. The pure molybdenum colloid reveals diffraction peaks of molybdenum, as well as for molybdenum oxide (MoO_2). The diffraction patterns of the mixed colloid contain characteristic peaks for molybdenum and nickel.

It is noticeable, that a gradual peak shift of the nickel diffraction peaks, corresponding to the {111} and {200} pattern toward larger 2-θ was measured with increased molar fraction of molybdenum. The nickel lattice constant increases with a higher amount of molybdenum, corresponding to a lattice expansion of nickel due to tensile stress (Figure 6). This can be explained by the diffusion of the larger molybdenum atoms (136.2 pm) in the fcc lattice with the smaller nickel atoms (124.6 pm). On the other hand, the molybdenum x-ray peaks {110}, {200} do not shift, indicating nickel does not diffuse into molybdenum noticeable. With the lattice constant, one can estimate the concentration of molybdenum solved in nickel

lattice according to equation (Eq.1), which is also plotted in Figure 6 [47]. The calculated concentration of molybdenum in the nickel lattice is below the maximum soluble concentration of 13 At. % (at room temperature), which shows that a diffusion into the nickel lattice is possible [47]. The crystallite size of the molybdenum and nickel nanoparticles was calculated from Scherrer's equation for full width at half maximum (FWHM) of {111} and {200} reflections. A significant decrease of the crystallite size was found with increased feeding of molybdenum, indicating higher electro catalytic performance [48].

$$Mo - portion\ [At.\%] = \frac{a_{Ni(ss)} - a_{Ni}}{0{,}000409} \quad \text{(Eq.1)}$$

$a_{Ni(ss)}$ = lattice constant according to Eq. 1

a_{Ni} = lattice constant of nickel bulk (3,52394 Å)

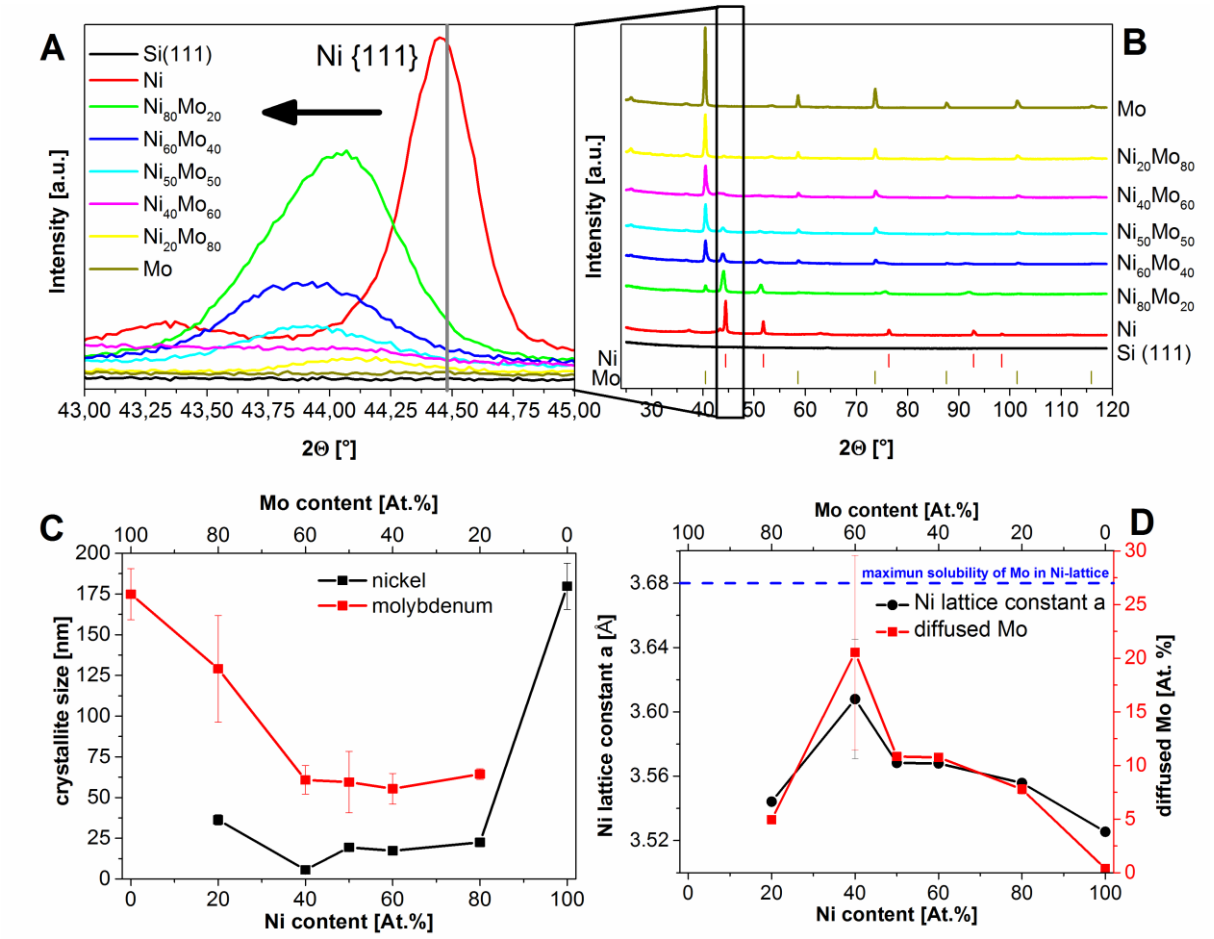

Figure 6: A) X-ray diffraction {111} peak shift of nickel in pure Ni and NiMo-colloids. B) XRD profiles of pure Ni, Mo and NiMo colloids. C) crystallite size, D) lattice constant and the content of diffused Mo in the Ni lattice as a function of Ni and Mo content.

Preliminary electrochemical measurements were carried out, using cyclic voltammetry the pure colloids molybdenum and nickel, as well as with $Ni_{40}Mo_{60}$ nanoparticles (Figure 7). In the voltammograms of all colloids hydrogen evolution was measured at low potentials in the range of -300 to -900 mV. The bubble formation leads to a rising cathodic current, with a shape of a peak, according to equation Eq.2 [49] [50] [51].

At the first cycle, nickel does not show any pronounced peaks. A small peak in the range of -0.1 mV to 0.2 mV can be observed, which can be attributed to the phase transition of α-nickel hydroxide to β-nickel hydroxide according to equation (Eq.3) [51].

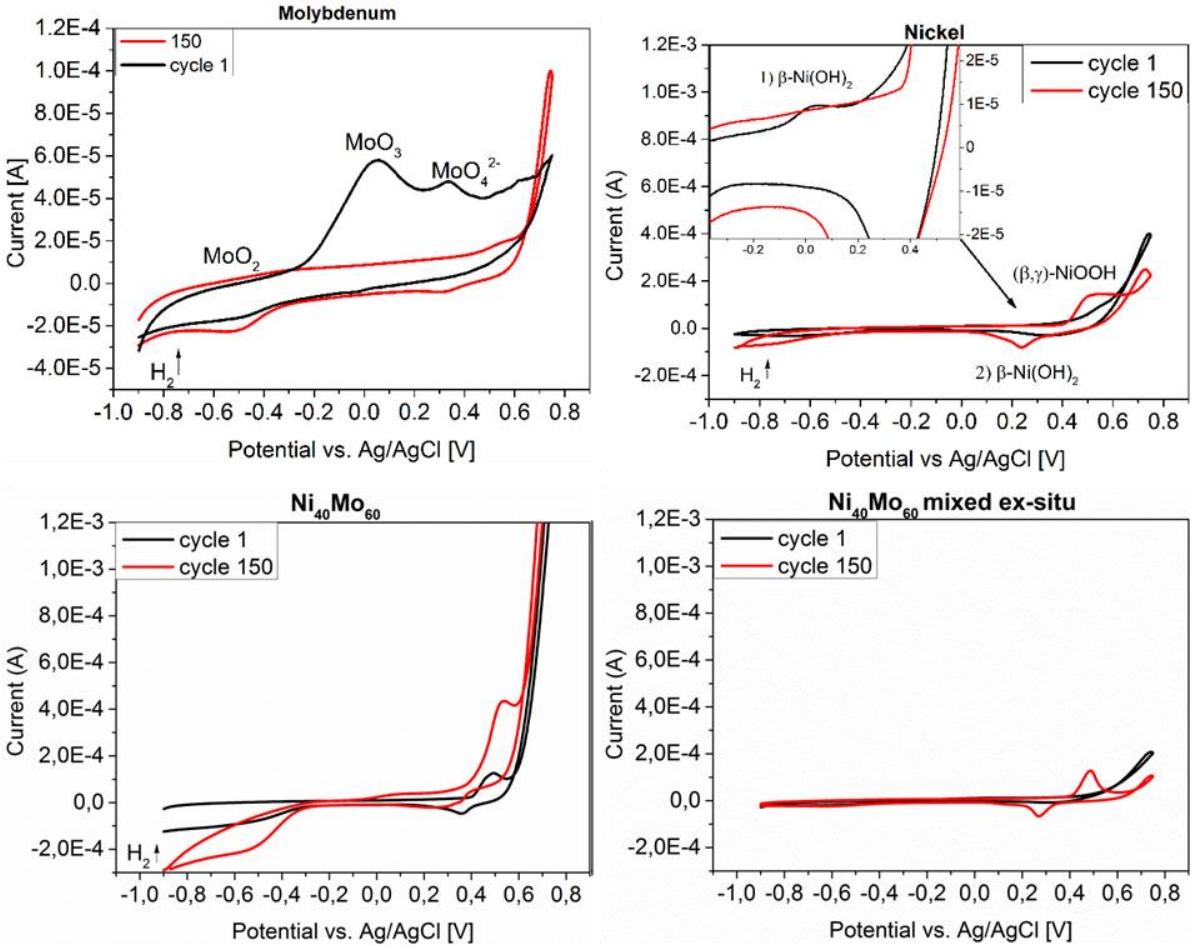

Figure 7: Cyclic voltammograms of pure molybdenum and nickel colloid, as well as of nickel-molybdenum colloids synthesized in-situ and of mixed ex-situ nickel-molybdenum colloid.

By increased cycles, anodic currents at 380 mV-750 mV appears, corresponding to the oxidation of Ni(II) to Ni(III), which is due to the formation of nickel oxyhydroxides (Eq.4) [52] [51]. The appearance of a cathodic peak at 60 mV- 390mV shows a quasi-reversible reaction to nickel hydroxide [53].

(Eq.2) $2H_2O + 2e^- \rightarrow 2OH^- + H_2$

(Eq.3) $\alpha Ni(OH)_2 \rightarrow \beta Ni(OH)_2$

(Eq.4) $\beta Ni(OH)_2 + OH^- \rightarrow (\beta,\gamma)NiOOH + H_2O + e^-$

Molybdenum reveals at the first cycle clearly anodic peaks at -250-200 mV (Peak at 45 mV), 200-450 mV (peak at 330 mV) and 45-670 mV (peak at ≈ 620 mV) vs. Ag/AgCl-reference electrode. At the cathodic scan, no peaks can be observed, indicating that irreversible reactions takes place. These anodic peaks can be attributed to the formation of

(Eq.5) $Mo + 4OH^- \rightarrow MoO_2(s) + 2H_2O + 4e^-$

(Eq.6) $MoO_2 + 2OH^- \rightarrow MoO_3(s) + H_2O + 2e^-$

(Eq.7) $MoO_3 + 2OH^- \rightarrow MoO_4^{2-} + H_2O$

molybdenum oxide with subsequent oxidation steps [50] [54]. The formation of MoO_2 and further oxidation to MoO_3 can be represented by equations (Eq.5) and (Eq.6) [49]. At higher potentials MoO_3 can be dissolved to Mo (VI), which explain, that no reduction takes place on the electrode (Eq.7). The following scans showed no further oxidation peaks, meaning that the oxidation of molybdenum is irreversible, because no subsequent reactions appear. The reproducibility of the peak intensity of colloids containing molybdenum is not feasible, because ongoing change in the composition of various molybdenum species is caused due to exposure to light, which was discussed above.

Compared with $Ni_{40}Mo_{60}$ colloidal solution, which was prepared ex-situ by mixing the pure colloids in the corresponding molar ratio, the cyclic voltammogram of the in-situ prepared $Ni_{40}Mo_{60}$ colloid shows a stronger current change in the hydrogen evolution region, indicating a higher electrocatalytic activity. It should be noted, the recorded cyclic voltammograms changing their shape by reproducing the measurements, but the trend is still maintained. Cyclic voltammorams of $Ni_{40}Mo_{60}$ (in-situ and ex-situ) showing the same shape as for pure nickel colloid. Though similar voltammograms were obtained, Krstajic et al. has shown that Ni-Mo alloys exhibit better activity towards hydrogen evolution reaction than pure nickel [53]. Just by considering the cyclic voltammograms of the nanoparticles, it is not possible to conclude to their full electrochemical behaviour and activity. Therefore further electrochemical investigations, has to be done in order to obtain more specifications on the electrochemical behaviour of the nickel-molybdenum nanoparticles.

Conclusion

We fabricated ligand-free and purely electrostatically stabilized nickel-molybdenum nanoparticles by pulsed laser ablation in water. For this purpose, ablation targets of desired composition were formed by pressing and subsequent sintering of mixed nickel and molybdenum micro powders. The colloids resulting from laser ablation show a formation of mixed nanoparticles even though a controlled stoichiometry by adjusting the target composition could not be shown by TEM-EDX. However, XRD analysis reveal that the properties of the colloidal nanoparticles changed by modifying the target's composition. A significant lattice strain for nickel, due to a diffusion of molybdenum into the nickel lattice, was found in the molybdenum rich colloids, resulting in smaller crystallites, which represent a promising material for electro-catalysis. Molybdenum rich systems tend to a formation of molybdenum oxides, which were also confirmed by electrochemical investigations. Cyclic voltammograms show typically irreversible oxidation peaks for molybdenum nanoparticle. Nickel nanoparticles reveal significant anodic and cathodic currents, due to a quasi-reversible oxidation of Ni(II) to Ni(III).

Literature

[1] D. Tiedemann, U. Taylor, C. Rehbock, J. Jakobi, S. Klein, W. A. Kues, S. Barcikowski, and D. Rath, *Analyst*, vol. 139, pp. 931–942, 2014.

[2] J. A. Rodriguez and D. W. Goodman, *Science*, vol. 257, no. 5072, pp. 897–903, 1992.

[3] M. Oezaslan, M. Heggen, and P. Strasser, *Journal of the American Chemical Society*, vol. 134, no. 1, pp. 514–524, 2011.

[4] A. Freund, J. Lang, T. Lehmann, and K. A. Starz, *Catalysis Today*, vol. 27, no. 1, pp. 279–283, 1996.

[5] P. Strasser, *Reviews in Chemical Engineering*, vol. 25, no. 4, pp. 255–295, 2009.

[6] F. Hasché, M. Oezaslan, and P. Strasser, *Physical Chemistry Chemical Physics*, vol. 12, no. 46, pp. 15251–15258, 2010.

[7] C. Song, *Catalysis Today*, vol. 77, pp. 17–49, 2002.

[8] J. T. M. M. H. A. D. Peter M. Urban, Anett Funke, *Applied Catalysis A: General*, vol. 221, pp. 459–470, 2001.

[9] G. Acres, J. Frost, G. Hards, R. Potter, T. Ralph, D. Thompsett, G. Burstein, and G. Hutchings, *Catalysis Today*, vol. 38, no. 4, pp. 393–400, 1997.

[10] H. A. Gasteiger, S. S. Kocha, B. Sompalli, and F. T. Wagner, *Applied Catalysis B: Environmental*, vol. 56, no. 1, pp. 9–35, 2005.

[11] N. Tian, Z.-Y. Zhou, S.-G. Sun, Y. Ding, and Z. L. Wang, *science*, vol. 316, no. 5825, pp. 732–735, 2007.

[12] W. Sheng, H. A. Gasteiger, and Y. Shao-Horn, *Journal of The Electrochemical Society*, vol. 157, no. 11, pp. B1529–B1536, 2010.

[13] M. G. Walter, E. L. Warren, J. R. McKone, S. W. Boettcher, Q. Mi, E. A. Santori, and N. S. Lewi, *Chem. Rev.*, vol. 110, pp. 6446–6473, 2010.

[14] S. Trasati, *J. Electroanal. Chem.*, vol. 39, pp. 163–184, 1972.

[15] M. H. Miles, *Journal of Electroanalytical Chemistry and Interfacial Electrochemistry*, vol. 60, pp. 89–96, 1975.

[16] F. Mafune, J. Kohno, Y. Takeda, and T. Kondow, *J. Phys. Chem. B*, vol. 106, pp. 8555–8561, 2002.

[17] G. Compagnini, A. Scalisi, and O. Puglisi, *Journal of applied physics*, vol. 94, no. 12, pp. 7874–7877, 2003.

[18] Y. Kimura, H. Takata, M. Terazima, T. Ogawa, and S. Isoda, *Chemistry Letters*, vol. 36, no. 9, pp. 1130–1131, 2007.

[19] T. Tsuji, K. Iryo, N. Watanabe, and M. Tsuji, "Preparation of silver nanoparticles by laser ablation in solution: influence of laser wavelength on particle size," *Appl. Surf. Sci.*, vol. 203, pp. 80–85, 2002.

[20] S. Barcikowski, A. Hahn, A. V. Kabashin, and B. Chichkov, *Appl. Phys. A*, vol. 87(1), p. 47–55, 2007.

[21] J. Zhang, D. N. Oko, S. Garbarino, R. Imbeault, M. Chaker, A. C. Tavares, D. Guay, and D. Ma, *J. Phys. Chem. C*, vol. 116, pp. 13413–13420, 2012.

[22] S. Barcikowski, F. Devesa, and K. Moldenhauer, *J. Nanopart. Res.*, vol. 11, pp. 1883–1893, 2009.

[23] S. Barcikowski and G. Compagnini, *Phys. Chem. Chem. Phys.*, vol. 15, pp. 3022–3026, 2013.

[24] D. Kil, Y. Suh, H. Jang, J. Lee, C. Song, and W. Kim, *Materials transactions*, vol. 46, no. 11, pp. 2509–2513, 2005.

[25] K. Nouneh, M. Oyama, R. Diaz, M. Abd-Lefdil, I. Kityk, and M. Bousmina, *Journal of Alloys and Compounds*, vol. 509, no. 19, pp. 5882–5886, 2011.

[26] K. Chandrappa, T. Venkatesha, K. Nayana, and M. Punithkumar, *Materials and Corrosion*, vol. 63, no. 5, pp. 445–455, 2012.

[27] J. A. Creighton and D. G. Eadont, *J. Chem. Soc. Faraday Trans.*, vol. 87, pp. 3881–3891, 1991.

[28] K. Krishnamoorthy, M. Veerapandian, K. Yun, and S. J. Kim, *Colloids and Surfaces B: Biointerfaces*, vol. 112, pp. 521–524, 2013.

[29] H. Sinaim, A. Phuruangrat, S. Thongtem, and T. Thongtem, *Materials Chemistry and Physics*, vol. 132, no. 2, pp. 358–363, 2012.

[30] J. Cruywagen and J. Heyns, *Inorganic Chemistry*, vol. 26, no. 16, pp. 2569–2572, 1987.

[31] R. S. Weber, *Journal of Catalysis*, vol. 151, no. 2, pp. 470–474, 1995.

[32] T. He and J. Yao, *Journal of Photochemistry and Photobiology C: Photochemistry Reviews*, vol. 4, no. 2, pp. 125–143, 2003.

[33] L. Zheng, Y. Xu, D. Jin, and Y. Xie, *Chemistry of Materials*, vol. 21, no. 23, pp. 5681–5690, 2009.

[34] G. Cristoforetti, E. Pitzalis, R. Spiniello, R. Ishak, and M. Muniz-Miranda, *J. Phys. Chem. C*, vol. 115, p. 5073–5083, 2011.

[35] V. Amendola and M. Meneghetti, *Phys. Chem. Chem. Phys.*, vol. 15, pp. 3027–3046, 2013.

[36] W. T. Nichols, T. Sasaki, and N. Koshizaki, *J. Appl. Phys.*, vol. 100, p. 114912, 2006.

[37] M. S. I. Sarker, T. Nakamura, Y. Herbani, and S. Sato, *Applied Physics A*, vol. 110, no. 1, pp. 145–152, 2013.

[38] M. S. Islam Sarker, T. Nakamura, and S. Sato, *Journal of Materials Research*, vol. 29, no. 07, pp. 856–864, 2014.

[39] K. Yuge, *Physical Review B*, vol. 84, no. 8, p. 085451, 2011.

[40] J. Koch, A. Von Bohlen, R. Hergenröder, and K. Niemax, *Journal of Analytical Atomic Spectrometry*, vol. 19, no. 2, pp. 267–272, 2004.

[41] L. J. Lewis and D. Perez, *Applied Surface Science*, vol. 255, no. 10, pp. 5101–5106, 2009.

[42] H. Dang, Z. Han, Z. Dai, and Q. Qin, *International journal of mass spectrometry*, vol. 178, no. 3, pp. 205–212, 1998.

[43] A. Neumeister, J. Jakobi, C. Rehbock, J. Moysig, and S. Barcikowski, *Phys. Chem. Chem. Phys.*, pp. –, 2014.

[44] J. Jakobi, A. Menendez-Manjon, V. S. K. Chakravadhanula, L. Kienle, P. Wagener, and S. Barcikowski, *Nanotechnology*, vol. 22, p. 145601, 2011.

[45] J. Jakobi, S. Petersen, A. Menendez-Manjon, P. Wagener, and S. Barcikowski, *Langmuir*, vol. 26, p. 6892–6897, 2010.

[46] Y. Ishikawa, K. Kawaguchi, Y. Shimizu, T. Sasaki, and N. Koshizaki, *Chemical physics letters*, vol. 428, no. 4, pp. 426–429, 2006.

[47] R. Schulz, J. Huot, M. Trudeau, L. Dignard-Bailey, Z. Yan, S. Jin, A. Lamarre, E. Ghali, and A. Van Neste, *Journal of materials research*, vol. 9, no. 11, pp. 2998–3008, 1994.

[48] P. Strasser, S. Koh, T. Anniyev, J. Greeley, K. More, C. Yu, Z. Liu, S. Kaya, D. Nordlund, H. Ogasawara, *et al.*, *Nature Chemistry*, vol. 2, no. 6, pp. 454–460, 2010.

[49] W. Badawy, H. Feky, N. Helal, and H. Mohammed, *International Journal of Hydrogen Energy*, vol. 38, no. 23, pp. 9625–9632, 2013.

[50] F. Endres and G. Schwitzgebel, *Journal of Electroanalytical Chemistry*, vol. 415, no. 1, pp. 23–26, 1996.

[51] M. Dmochowska and A. Czerwinski, *Journal of Solid State Electrochemistry*, vol. 2, no. 1, pp. 16–23, 1998.

[52] M. R. O. Riyanto and J. Salimon, *Malaysian Journal of Analytical Sciences*, vol. 11, no. 2, pp. 379–387, 2007.

[53] N. Krstajic, V. Jovic, L. Gajic-Krstajic, B. Jovic, A. Antozzi, and G. Martelli, *Ínternational Journal of Hydrogen Energy*, vol. 33, no. 14, pp. 3676–3687, 2008.

[54] T. Heumann and M. Klimmeck, *Materials and Corrosion*, vol. 22, no. 2, pp. 115–120, 1971.